


Article

# Corrosion and Tribocorrosion Behaviors for TA3 in Ringer's Solution after Implantation of Nb Ions

Chenfei Xue <sup>1,2</sup>, Pingze Zhang <sup>1,2,\*</sup>, Dongbo Wei <sup>1,2,3</sup> , Hengmei Hu <sup>1,2</sup>, Fengkun Li <sup>1,2</sup> and Kai Yang <sup>1,2</sup>

<sup>1</sup> College of Materials Science and Technology, Nanjing University of Aeronautics and Astronautics, Nanjing 211106, China; xuechenfei@nuaa.edu.cn (C.X.); weidongbo@nuaa.edu.cn (D.W.); hhm@nuaa.edu.cn (H.H.); lifengkun@nuaa.edu.cn (F.L.); ykcl@nuaa.edu.cn (K.Y.)

<sup>2</sup> Materials Preparation and Protection for Harsh Environment Key Laboratory of Ministry of Industry and Information Technology, Nanjing 211106, China

<sup>3</sup> Aero-engine Thermal Environment and Structure Key Laboratory of Ministry of Industry and Information Technology, Nanjing 211106, China

\* Correspondence: zhangpingze@nuaa.edu.cn; Tel.: +86-139-5188-3686

Received: 1 November 2020; Accepted: 21 November 2020; Published: 24 November 2020



**Featured Application:** A potential application of this work is in the corrosion and tribocorrosion behaviors of Ti alloys after surface modification.

**Abstract:** Ti alloys are prone to corrosion and wear due to the hostile environment in bodily fluids, but the Ti-45Nb alloy is considered to be a promising titanium alloy with excellent biocompatibility and resistance to physiological corrosion. In this study, Nb ions were implanted into a TA3 alloy and the effect on the biological corrosion as well as tribocorrosion behavior of TA3 in Ringer's solution was systematically investigated. The surface microstructure and XRD results revealed that the implanted samples showed a smoother surface due to the sputtering and radiation damages, and the Nb ions mainly existed in the alloy as the solid solution element. The electrochemical polarization tests showed that the implantation of Nb ions can increase the corrosion potential of the samples, showing a better thermodynamic stability. The tribocorrosion tests showed that the implanted samples exhibited a better thermodynamic stability in a corrosive environment accompanied by wear behavior, and the worn surface showed fewer pitting pits, indicating a better corrosion resistance. However, the abrasive wear and oxidation wear degree of the sample increased because of partial softening of the surface and brittle passivation film.

**Keywords:** TA3; ion implantation; corrosion resistance; tribocorrosion resistance; Ringer's solution

## 1. Introduction

Titanium and its alloys have been considered as some of the most suitable implants for the replacement and repair of human hard tissues because of their good corrosion resistance, mechanical properties and biocompatibility [1–4]. Among the various titanium alloys, Ti-6Al-4V and Ti-6Al-7Nb have been widely used owing to their good properties [3,5,6]. However, they are easy to dissolve and can undergo aseptic loosening in physiological environments due to the complex electrolyte environment in human bodily fluids, as well as the comprehensive action of active cells [2,5]. Furthermore, some studies have revealed that the corrosion and wear behavior of Ti-6Al-4V leads to the diffusion of aluminum and vanadium into the blood, causing local inflammation, allergies, poisoning, and diseases such as Alzheimer's disease [6,7]. In addition, the two-phase ( $\alpha+\beta$ ) Ti-6Al-4V has poorer corrosion resistance than the single-phase due to the galvanic coupling effect [8]. Therefore, there has been

a continuing interest in exploring new materials with excellent properties and no toxicity. Surface modification treatment on existing materials is a feasible solution.

Ion implantation is a surface modification technique, in which high-energy ion beams are implanted onto the surface of a material and eventually remain inside to optimize the surface performance [9]. At present, ion implantation has been widely used in the surface modification of Ti and its alloys in the medical field [10–14]. Yan et al. [13] implanted Zr ions into a titanium surface and revealed that a Ti–Zr alloy layer on titanium exhibited good mechanical properties and corrosion resistance. Zhao et al. [15] observed that the generation of Nb<sub>2</sub>O<sub>5</sub>/TiO<sub>2</sub> and implanting Nb ions into a Ni–Ti alloy significantly improved the corrosion resistance of the composite film in Hank's solution. Zu et al. [16] implanted Nb ions to obtain a wear-resistant modified layer in Ti–Al–Zr, and the wear-resistance improved because of the formation of intermetallic NbTi<sub>4</sub>. Studies have shown that the presence of Nb can stabilize the passivated film of Ti alloys, improve the corrosion resistance, and improve its wear-resistance [15,17].

Titanium alloys are prone to corrosion and wear phenomena coming from the hostile environment of the body and friction processes, and sometimes the wear and corrosion behaviors of titanium alloys occur simultaneously when used as an implant material. Therefore, it is necessary to study the tribocorrosion problem in bodily fluids while studying corrosion behavior, as it is more meaningful for practical application and provides data references for practical application.

In this paper, Nb ions were implanted into the single-phase TA3 with a dose of  $6.85 \times 10^{16}$  ions/cm<sup>2</sup> at an energy of 125 keV. The surface morphology, phase structure, mechanical properties, corrosion and tribocorrosion behavior of the samples in Ringer's solution were characterized by scanning electron microscopy (SEM), X-ray diffraction (XRD), friction and wear instrument and nanoindentation instrument, combined with electrochemical measurements.

## 2. Experimental Details

### 2.1. Test Specimens and Ion Implantation

The pure titanium TA3 was cut into block samples of 15 mm × 15 mm × 4 mm. Prior to Nb ion implantation, the samples were prepared by standard metallographic technique to the extent that the surface roughness was below 0.2 μm. Following this, they were polished to a mirror finish with a silica suspension, washed by ultrasonic in anhydrous ethanol and finally dried in air. Niobium (Nb, 99.99 wt%) ions were injected at an extraction voltage of 125 keV and a vacuum of 10<sup>−3</sup> Pa with a dose of  $6.85 \times 10^{16}$  ions/cm<sup>2</sup>.

### 2.2. Surface Characterization and Crystal Structure Analysis

The usage of scanning electron microscopy (SEM) and X-ray diffraction (XRD) was to observe the change of surface morphology and the phase composition of samples after they were injected, while the composition distribution on the surface of samples was determined by EDS.

### 2.3. Characterization of Mechanical Properties

The nanoindentation instrument (DuH-W201) can be used to reflect the mechanical properties of the sample surface. In this paper, the static load control mode was selected with a loading load of 10 mN kept for 10 s, and the Load–Displacement curves were obtained. The average values were calculated from five different test points selected on each sample.

### 2.4. Electrochemical Test

A classical three-electrode system was utilized for electrochemical measurement, in which the reference electrode is a Saturated Calomel Electrode (SCE), the counter electrode is a platinum electrode, and the working electrode is the specimen. All the samples were coated with AB glue, except for an exposed area of 1 cm<sup>2</sup> soaked in Ringer's solution at 37 °C for electrochemical testing. The constituents of Ringer's solution were NaCl 8.61 g/L, CaCl<sub>2</sub> 0.49 g/L and KCl 0.30 g/L. After a stable open circuit

potential (OCP), the potentiodynamic polarization was conducted from  $-0.8$  V to  $0.8$  V with a scan rate of  $1$  mV/s. All the measurements were carried out by the ZAHNER ZENNIUM.

### 2.5. Tribocorrosion Tests

The tribocorrosion behavior of samples was studied by using a reciprocating tribometer. Sliding wear conditions against GCr15 steel balls with a diameter of  $6$  mm were established in Ringer's solution. The performed load was  $2$  N, and the friction test reciprocating length was  $5$  mm with a frequency of  $1$  Hz for  $10$  min. In this test, the curves of open circuit potential as well as the coefficient of friction (COF) were recorded before, during and after the wear process, where the samples were immersed in Ringer's solution with an exposed area of  $1$  cm<sup>2</sup>. In addition, the SEM and 3D Measuring Laser Microscope were adopted to observe the morphology and measure the size of the worn surface.

## 3. Results and Discussion

### 3.1. Surface Structure and Morphology

The surface morphology and composition of TA3 before and after the implantation of Nb ions are shown in Figure 1. Compared to the substrate, the surface morphology of TA3 implanted with Nb ions appears smoother, while some small pits appear on the metal surface. Studies have suggested that some pits are formed on the surface due to the bombardment and cascade collisions caused by high-energy ion implantation [18,19]. Additionally, the etching effect produced during the continuous bombardment of TA3 with Nb ions reduces the relative height of the surface bulge, which explains the flattening of surface morphology [20]. In general, the smoother the surface, the better its corrosion resistance due to the smaller potential difference between the concave and convex [21,22]. Therefore, the effect of ion implantation on a metal's surface can improve the corrosion performance appropriately. Moreover, as shown in Figure 1, the content of Nb ions is approximately  $2.24$  at%, indicating that the Nb ions were implanted into the sample successfully. However, the content of Nb is lower, and this may be due to the far greater effective penetration depth of EDS than the implanted depth of Nb.

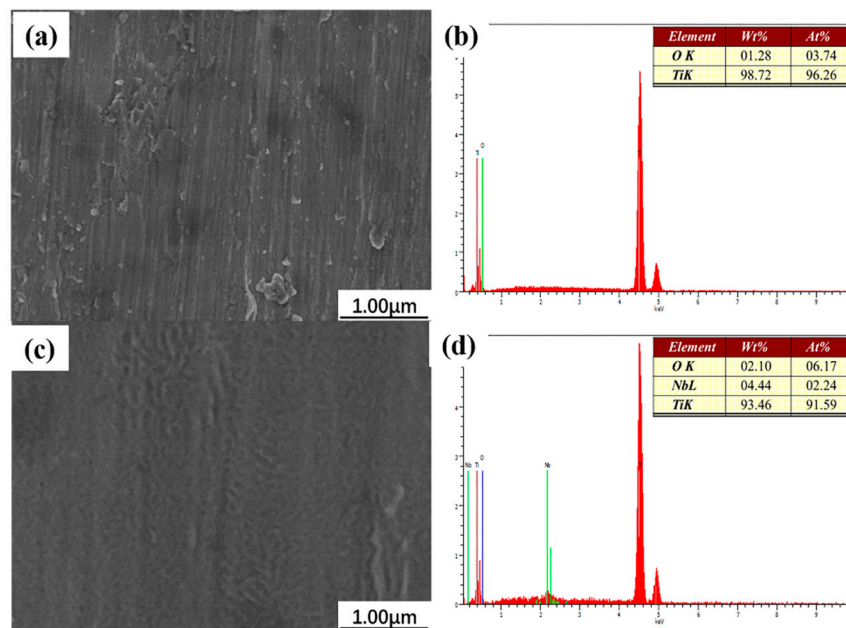


**Figure 1.** Backscattered SEM images and EDS analysis: (a,b) substrate, (c,d) Nb-implanted sample.

Figure 2 shows the XRD pattern of samples before and after Nb ions were implanted. Compared to the substrate, no new diffraction peaks were observed after Nb ions were implanted, indicating that

no new phase was formed and Nb ions mainly existed in the solid solution element, which would improve the mechanical properties of the metal surface owing to the solid solution intensification. Figure 2 shows that the diffraction peaks of Ti (101) and Ti (002) shifted towards the higher angle side after implantation. It is well known that the crystal imperfections resulting from ion implantation may lead to lattice distortion, leading to the shift of diffraction peaks [23]. As the ionic radius of Nb is greater than that of Ti, the implanted Nb ions occupy the position of Ti and may lead to localized compressive strain, explaining the shift direction of the diffraction peak. Different from tensile stress, the presence of residual compressive stress does not induce stress corrosion properties.

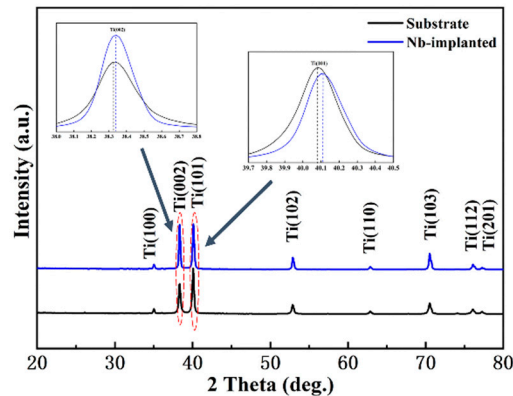


**Figure 2.** XRD patterns of substrate and the Nb-implanted sample.

### 3.2. Nanomechanical Properties

Figure 3 shows the Load–Displacement curves of nanoindentation tests for samples under 10 mN normal load. Table 1 shows the mechanical properties obtained by the L–D plots. In general, a higher ratio between hardness and elastic modulus ( $H/E$ ) serves as a better wear-resistance [24]. In this test, the elastic modulus ( $E$ ) and hardness ( $H$ ) of the implanted samples decreased to 78% and 61.7% of the substrate, respectively. In addition, the  $H/E$  was approximately 78% of the substrate. Studies have shown that the irradiation effect during the implantation may increase the surface temperature of the samples, causing the substrate to soften [25]. The associated bombardment and cascade collisions will form a large number of defects on the surface, such as vacancy, dislocation and dislocation group, strengthening the substrate to some extent.

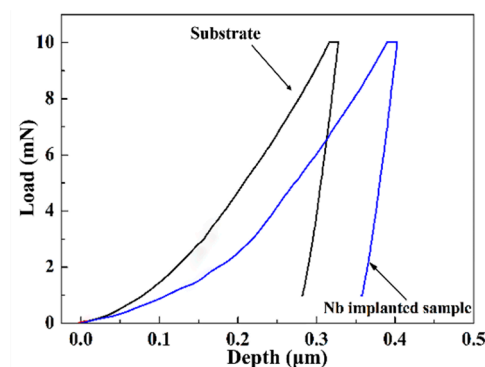


**Figure 3.** The nanoindentation Load–Displacement curves of the substrate and the Nb-implanted sample.

**Table 1.** Calculated values of elastic modulus and hardness of samples.

Sample	H(GPa)	E(GPa)	H/E
substrate	4.677	146.645	0.032
Nb implanted	2.888	114.743	0.025

### 3.3. Corrosion Performance

Figure 4 shows the potentiometric polarization results of the samples immersed for 1 h at 37 °C in Ringer's solution, in which the anode branch represents the dissolution of the Ti under higher potential, whereas the cathode branch represents the hydrogen evolution reaction [26]. It can be seen in Figure 4 that Nb ion implantation shifted the anode part towards positive potential, and areas of passivation can be observed obviously, which indicates that the implanted samples have better thermodynamic stability. In addition, the results present a higher slope in the anode part than in the cathode part, indicating that the corrosion process is controlled by the anodic process (active dissolution of the metal) and is conducive to inhibiting the dissolution of Ti alloys [27].

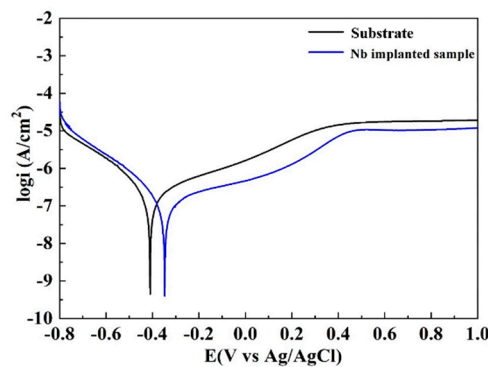


**Figure 4.** The potentiodynamic polarization curves of the untreated and treated samples in Ringer's solution.

Table 2 shows the electrochemical parameters obtained, including corrosion potential ( $E_{\text{corr}}$ ), corrosion current density ( $I_{\text{corr}}$ ) and polarization resistance ( $R_p$ ) from the Tafel plots. The results clearly show that, compared with the substrate, the  $E_{\text{corr}}$  of implanted samples increased by 0.15 V, and the  $I_{\text{corr}}$  also decreased by an order of magnitude. In addition, the  $R_p$  of the implanted samples is about three times as much as that of the substrate. Additionally, it can be observed that the implanted sample has a lower passivation current, which indicates that the passivation layer of the implanted sample has a better corrosion resistance. The above results show that Nb ion modification can effectively improve the thermodynamic and kinetic stability of the passivation layer, exhibiting a better corrosion protection effect in the short-term immersion.

**Table 2.** Corrosion parameters calculated from the potentiodynamic polarization curves.

Sample	$E_{\text{corr}}$ (V)	$I_{\text{corr}}$ ( $\mu\text{A}/\text{cm}^2$ )	$R_p$ ( $\text{k}\Omega/\text{cm}^2$ )
Substrate	-0.349	0.194	340
Nb implanted	-0.199	0.051	1110

### 3.4. Tribocorrosion Tests

The tribocorrosion tests (combined corrosion and wear tests) were performed according to the experimental procedure described in Section 2.5. The variation in the coefficient of friction (COF) and open circuit potential (OCP) of substrates and Nb-implanted samples is shown in Figure 5. In general, the friction coefficient will vary with the degree of surface damage and wear. Starting load at after 5 min, the COF of the substrate increases rapidly and enters the stable wear stage with an average friction coefficient of 0.395, while that of the Nb-implanted sample remains around 0.15 at the initial stage of wear due to the reduced surface roughness of the sample caused by ion implantation. However, it increases sharply and becomes similar to that of the substrate after about 2 min, which may be due to wear of the implanted layer and the exposure of the substrate as wear deepens.

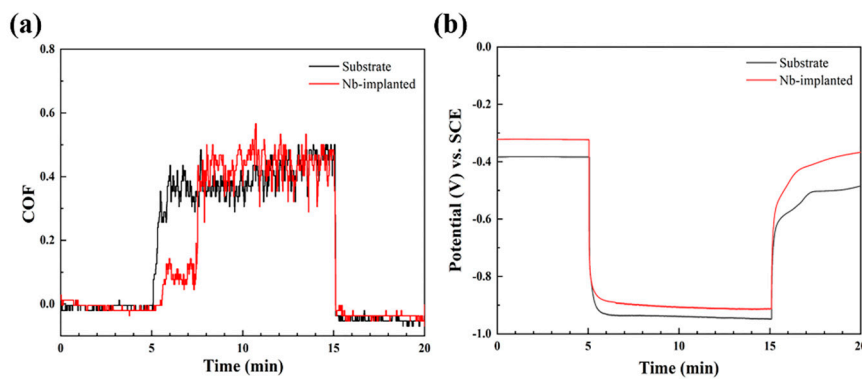
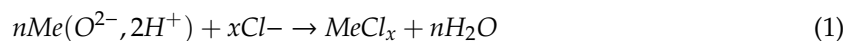


**Figure 5.** The variation of coefficient of friction and open circuit potential of samples in Ringer's: (a) coefficient of friction; (b) open circuit potential.

In general, the variation in the OCP is affected by friction and dielectric corrosion [28]. It can be observed in Figure 5b that the OCP of both samples reaches a steady state after 5 min of immersion in Ringer's and before the tribological process, indicating the formation of a stable passivation film. The OCP of samples mutates and moves towards a lower potential due to local damage to the passivation film of the worn surface after a tribological load. The exposed inner metal is more prone to corrosion due to the wear behavior. In addition, the agitation in the friction process promotes the corrosion reaction, which explains the mutation of the OCP. After unloading the load, the OCP of both samples increases rapidly and gradually becomes stable because the metal at the abrasion mark being exposed to the solution promotes the formation of a new passive layer. The presence of defects at the wear marks decreases the OCP to a lower level than it was before the load. It can be observed that the potential of the implanted sample becomes stable faster and is higher than that of the substrate, which indicates that Nb can still improve the corrosion behavior of the substrate after the wear behavior. The OCP of the implanted samples is higher than that of the substrate before, during, and after the wear process, indicating that the implantation of Nb ions can reduce the corrosion sensitivity and improve corrosion resistance.

The morphology and element composition of the wear scar were tested and shown in Figure 6. A certain number of grooves were seen on the wear scar because the wear debris are repeatedly rolled and embedded into the substrate surface. This is a typical feature of abrasive wear. Many cracks and pitting pits were observed on the surface of the wear scar, indicating that corrosion wear occurred. Where cracks and pitting occur, there is a high corrosion tendency [29]. The elemental composition in Figure 6c shows that the surface of the wear scar is mainly composed of elements Ti, O and Cl. When the oxide film ruptures during tribocorrosion, Cl ions diffuse easily along the defect and thus form soluble chlorine salts. In addition, the corrosion effect of Ringer's solution accelerates the initiation and propagation of cracks and finally leads to the shedding of wear debris, thus forming pitting pits, following Equation (1):



where  $Me(O^{2-}, 2H^+)$  represents the metal oxide film in solution and  $MeCl_x$  is the soluble chlorine salt. In addition, the heat generated in the wear process will promote the oxidation reaction. Brittle oxide film is more likely to break under the action of wear, and its repeated breaking and repair accelerate the wear of the substrate.

Compared to the substrate, Figure 6d–f show that the cracks and pitting pits in the wear scar are obviously less than that of the substrate, indicating a lower pitting tendency; however, the depth of the wear scar is greater than that of the substrate. One possible reason is that local softening of the Nb-implanted sample reduced the elastic and plastic deformation resistance, thus the wear debris has a more obvious ploughing effect on samples. Compared to the substrate, the Nb-implanted sample has a decreased content of O in the wear scar, and this may be because the faster rate of oxidation film



formation increases the wear in tribocorrosion. In addition, a small amount of the Nb element was observed in the wear scar, and its protective effect for the substrate is not completely lost as it explains the higher OCP of the implanted samples than that of the substrate after tribocorrosion. Figure 7 shows the three-dimensional contours and grinding crack profile of the sample. In addition, the calculation of wear volume shown in Table 3 reveals that the wear rate of the implanted sample is about 1.35 times that of the substrate, because the local softening effect of the implanted sample increases the wear debris during the wear process. Moreover, the Nb element accelerates the formation rate of the brittle passivation film, which is easy to break under the load, increasing the wear rate.

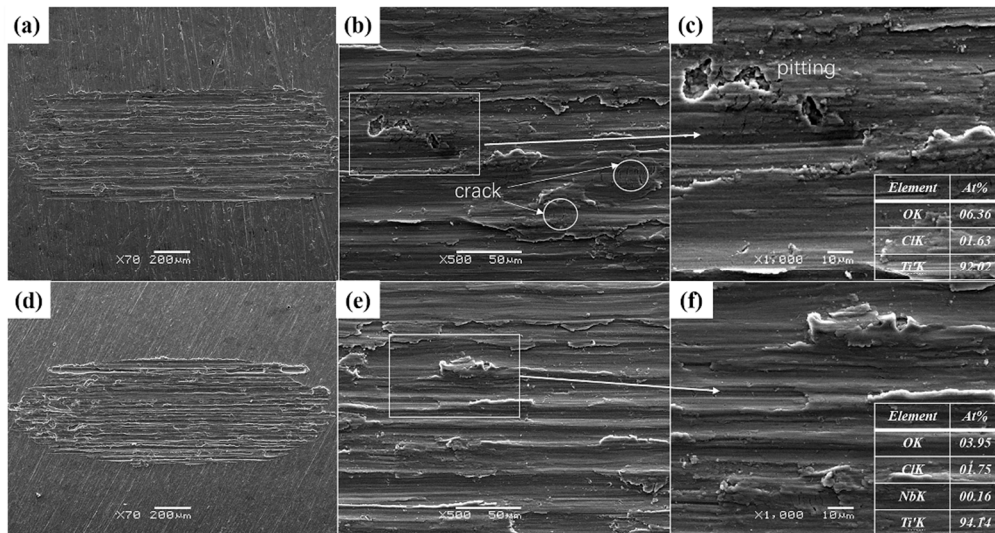


Figure 6. The worn surface and EDS analysis of samples: (a–c) substrate; (d–f) Nb-implanted sample.

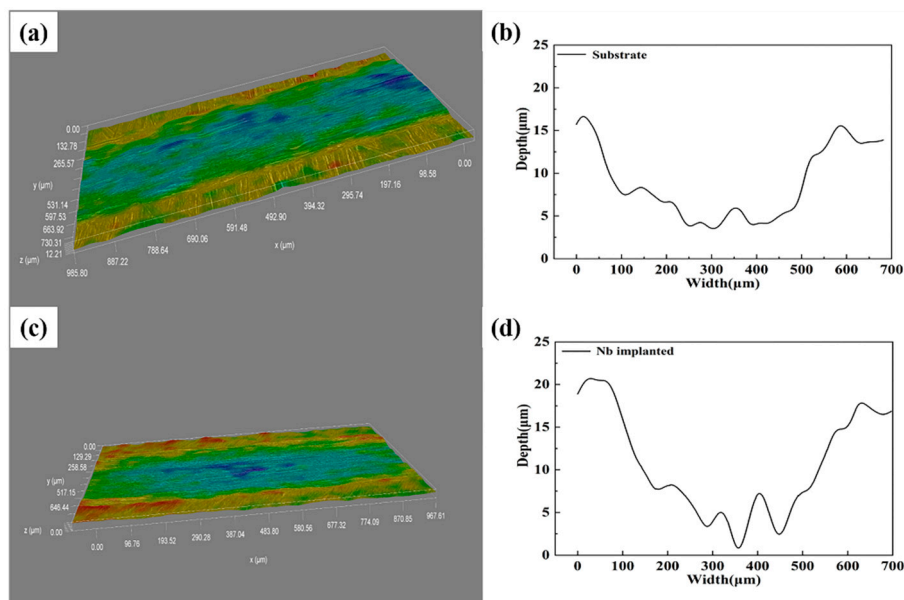


Figure 7. Three-dimensional contours and grinding crack profile of samples: (a,b) substrate; (c,d) Nb-implanted sample.

**Table 3.** Calculation results of wear scar of samples.

Sample	Width (μm)	Depth (μm)	Wear Volume (×10 <sup>-3</sup> mm <sup>3</sup> )	Wear Rate (×10 <sup>-4</sup> mm <sup>3</sup> N <sup>-1</sup> m <sup>-1</sup> )
Substrate	551.2	11.9	13.1	18.3
Nb implanted	539.2	16.5	17.8	24.8

#### 4. Conclusions

In this research, the corrosion resistance and tribocorrosion resistance in Ringer's physiological solution of TA3 implanted by Nb ions were systematically investigated. The observations of this study are as follows:

The implantation led to pits on the surface caused by irradiation damage and cascade collision, but it also made the surface smoother. The XRD patterns showed that Nb ions mainly exist in the form of a solid solution. The nanoindentation tests showed that elastic modulus and abrasion decrease because of the irradiation effect during implantation.

The potentiodynamic polarization curves revealed that the implanted samples indicated a higher corrosion potential and a lower current density, indicating that Nb ions can effectively improve the thermodynamic and kinetic stability of the passivation layer and promote the formation rate of passivation film.

The tribocorrosion tests showed that the ion implanted samples show better thermodynamic stability and can still display better corrosion behavior after the wear behavior. The morphology of the wear scar showed that the Nb-implanted sample has a lower pitting tendency, but due to the surface's partial softening and brittle passivation film, the abrasive wear and oxidation wear degree of the sample increased.

**Author Contributions:** Conceptualization, P.Z., C.X. and H.H.; methodology, H.H., C.X. and F.L.; validation, P.Z., D.W. and H.H.; formal analysis, P.Z., D.W., H.H. and C.X.; investigation, H.H., C.X., F.L. and K.Y.; resources, P.Z. and D.W.; data curation, P.Z., C.X. and H.H.; writing—original draft preparation, P.Z., C.X. and H.H.; writing—review and editing, P.Z., C.X. and H.H.; visualization, C.X. and H.H.; supervision, P.Z.; project administration, P.Z.; All authors have read and agreed to the published version of the manuscript.

**Funding:** This project was supported by the Natural Science Foundation for Excellent Young Scientists of Jiangsu Province, China (Grant No. BK20180068), the China Postdoctoral Science Foundation (Grant No. 2018M630555), Opening Project of Materials Preparation and Protection for Harsh Environment Key Laboratory of Ministry of Industry and Information Technology (Grant No. XCA20013-1).

**Conflicts of Interest:** The authors declare no conflict of interest.

#### References

1. Yang, K.; Zhou, C.; Fan, H.; Fan, Y.; Jiang, Q.; Song, P.; Fan, H.; Chen, Y.; Zhang, X. Bio-Functional Design, Application and Trends in Metallic Biomaterials. *Int. J. Mol. Sci.* **2017**, *19*, 24. [[CrossRef](#)] [[PubMed](#)]
2. Turcio-Ortega, D.; Rodil, S.E.; Muhl, S. Corrosion behavior of amorphous carbon deposit in 0.89% NaCl by electrochemical impedance spectroscopy. *Diam. Relat. Mater.* **2009**, *18*, 1360–1368. [[CrossRef](#)]
3. Alves, A.C.; Sendão, I.; Ariza, E.; Toptan, F.; Ponthiaux, P.; Pinto, A.M.P. Corrosion behaviour of porous Ti intended for biomedical applications. *J. Porous Mater.* **2016**, *23*, 1261–1268. [[CrossRef](#)]
4. Revie, R.W. *Uhlig's Corrosion Handbook*, 2nd ed.; Anti Corrosion Methods & Materials; Emerald Group Publishing Limited: Bingley, UK, 2000; Volume 47.
5. Tamilselvi, S.; Raman, V.; Rajendran, N. Corrosion behaviour of Ti–6Al–7Nb and Ti–6Al–4V ELI alloys in the simulated body fluid solution by electrochemical impedance spectroscopy. *Electrochim. Acta* **2006**, *52*, 839–846. [[CrossRef](#)]
6. Fojt, J. Ti–6Al–4V alloy surface modification for medical applications. *Appl. Surf. Sci.* **2012**, *262*, 163–167. [[CrossRef](#)]



7. Choe, H.-C.; Saji, V.S.; Ko, Y.-M. Mechanical properties and corrosion resistance of low rigidity quaternary titanium alloy for biomedical applications. *Trans. Nonferrous Met. Soc. China* **2009**, *19*, 862–865. [[CrossRef](#)]
8. Atapour, M.; Pilchak, A.L.; Frankel, G.S.; Williams, J. Corrosion behavior of  $\beta$  titanium alloys for biomedical applications. *Mater. Sci. Eng. C* **2011**, *31*, 885–891. [[CrossRef](#)]
9. Wu, G.; Li, P.; Feng, H.; Zhang, X.; Chu, P.K. Engineering and functionalization of biomaterials via surface modification. *J. Mater. Chem. B* **2015**, *3*, 2024–2042. [[CrossRef](#)]
10. Liu, Y.; Zu, X.; Tang, R.; Xiang, X.; Wang, L.; Ma, W. Role of tantalum and nickel ion implantation on corrosion resistance properties of a Ti–Al–Zr alloy. *Surf. Coat. Technol.* **2007**, *201*, 7538–7543. [[CrossRef](#)]
11. Thair, L.; Mudali, U.; Bhuvaneshwaran, N.; Nair, K.; Asokamani, R.; Raj, B. Nitrogen ion implantation and in vitro corrosion behavior of as-cast Ti–6Al–7Nb alloy. *Corros. Sci.* **2002**, *44*, 2439–2457. [[CrossRef](#)]
12. Shypylenko, A.; Pshyk, A.V.; Grzeskowiak, B.; Medjanik, K.; Peplinska, B.; Oyoshi, K.; Pogrebnyak, A.; Jurga, S.; Coy, E. Effect of ion implantation on the physical and mechanical properties of Ti–Si–N multifunctional coatings for biomedical applications. *Mater. Des.* **2016**, *110*, 821–829. [[CrossRef](#)]
13. Yan, B.; Tan, J.; Wang, D.; Qiu, J.; Liu, X. Surface alloyed Ti–Zr layer constructed on titanium by Zr ion implantation for improving physicochemical and osteogenic properties. *Prog. Nat. Sci.* **2020**. [[CrossRef](#)]
14. Cisternas, M.; Bhuyan, H.; Retamal, M.; Casanova-Morales, N.; Favre, M.; Volkmann, U.G.; Saikia, P.; Diaz-Droguett, D.; Mändl, S.; Manova, D.; et al. Study of nitrogen implantation in Ti surface using plasma immersion ion implantation & deposition technique as biocompatible substrate for artificial membranes. *Mater. Sci. Eng. C* **2020**, *113*, 111002. [[CrossRef](#)]
15. Zhao, T.; Li, Y.; Xiang, Y.; Zhao, X.; Zhang, T. Surface characteristics, nano-indentation and corrosion behavior of Nb implanted NiTi alloy. *Surf. Coatings Technol.* **2011**, *205*, 4404–4410. [[CrossRef](#)]
16. Zu, X.; Liu, Y.; Lian, J.; Liu, H.; Wang, Y.; Wang, L.; Ewing, R. Surface modification of a Ti–Al–Zr alloy by niobium ion implantation. *Surf. Coatings Technol.* **2006**, *201*, 3756–3760. [[CrossRef](#)]
17. Ji, P.; Li, B.; Chen, B.; Wang, F.; Ma, W.; Zhang, X.; Ma, M.; Liu, R. Effect of Nb addition on the stability and biological corrosion resistance of Ti–Zr alloy passivation films. *Corros. Sci.* **2020**, *170*, 108696. [[CrossRef](#)]
18. Wan, H.; Si, N.; Chen, K.; Wang, Q. Strain and structure order variation of pure aluminum due to helium irradiation. *RSC Adv.* **2015**, *5*, 75390–75394. [[CrossRef](#)]
19. Sumie, K.; Toyoda, N.; Yamada, I. Surface morphology and sputtering yield of SiO<sub>2</sub> with oblique-incidence gas cluster ion beam. *Nucl. Instrum. Methods Phys. Res. Sect. B Beam Interact. Mater. Atoms* **2013**, *307*, 290–293. [[CrossRef](#)]
20. Wei, D.; Li, F.; Li, S.; Wang, S.; Ding, F.; Tian, T.; Chen, X.; Yao, Z. Effect of Cr ion implantation on surface morphology, lattice deformation, nanomechanical and fatigue behavior of TC18 alloy. *Appl. Surf. Sci.* **2020**, *506*. [[CrossRef](#)]
21. Li, W.; Li, D. Influence of surface morphology on corrosion and electronic behavior. *Acta Mater.* **2006**, *54*, 445–452. [[CrossRef](#)]
22. Hong, T.; Nagumo, M. Effect of surface roughness on early stages of pitting corrosion of Type 301 stainless steel. *Corros. Sci.* **1997**, *39*, 1665–1672. [[CrossRef](#)]
23. Chen, X.-H.; Zhang, P.; Wei, D.-B.; Huang, X.; Ding, F.; Li, F.-K.; Dai, X.-J.; Wang, Z.-Z. Correlation between crystal structure and mechanical performance of Cr-implanted 300M high-strength steel using X-ray diffraction method. *J. Iron Steel Res. Int.* **2019**, *26*, 1106–1116. [[CrossRef](#)]
24. Leyland, A.; Matthews, A. On the significance of the H/E ratio in wear control: A nanocomposite coating approach to optimised tribological behaviour. *Wear* **2000**, *246*, 1–11. [[CrossRef](#)]
25. Tähtinen, S.; Moilanen, P.; Singh, B.; Edwards, D. Tensile and fracture toughness properties of unirradiated and neutron irradiated titanium alloys. *J. Nucl. Mater.* **2002**, *307*, 416–420. [[CrossRef](#)]
26. Wu, G.; Zhang, X.; Zhao, Y.; Ibrahim, J.M.; Yuan, G.; Chu, P.K. Plasma modified Mg–Nd–Zn–Zr alloy with enhanced surface corrosion resistance. *Corros. Sci.* **2014**, *78*, 121–129. [[CrossRef](#)]
27. Liu, W.; Li, M.-C.; Luo, Q.; Fan, H.-Q.; Zhang, J.-Y.; Lu, H.-S.; Chou, K.-C.; Wang, X.-L.; Li, Q. Influence of alloyed magnesium on the microstructure and long-term corrosion behavior of hot-dip Al–Zn–Si coating in NaCl solution. *Corros. Sci.* **2016**, *104*, 217–226. [[CrossRef](#)]

28. Bayón, R.; Igartua, A.; González, J.; De Gopegui, U.R. Influence of the carbon content on the corrosion and tribocorrosion performance of Ti-DLC coatings for biomedical alloys. *Tribol. Int.* **2015**, *88*, 115–125. [[CrossRef](#)]
29. Dearnley, P.A.; Dahm, K.L.; Çimenoglu, H. The corrosion–wear behaviour of thermally oxidised CP-Ti and Ti–6Al–4V. *Wear* **2004**, *256*, 469–479. [[CrossRef](#)]

**Publisher’s Note:** MDPI stays neutral with regard to jurisdictional claims in published maps and institutional affiliations.



© 2020 by the authors. Licensee MDPI, Basel, Switzerland. This article is an open access article distributed under the terms and conditions of the Creative Commons Attribution (CC BY) license (<http://creativecommons.org/licenses/by/4.0/>).